FUDMA Journal of Sciences (FJS)
ISSN online: 2616-1370
ISSN print: 2645 - 2944
Vol. 6 No. 1, March, 2022, pp 266 - 277
DOI: https://doi.org/10.33003/fjs-2022-0601-873

UNSTEADY CONVECTIVE COUETTE FLOW WITH HEAT SINK AND RADIATION EFFECTS

***Omokhuale E. and Jabaka M. L.**

Department of Mathematical Sciences, Federal University Gusau, P. M. B. 1001, Zamfara State, Nigeria.

*Corresponding authors' email: **emmanuelomokhuale@yahoo.com**

ABSTRACT

In this research, the effects of heat sink and radiation on unsteady hydromagnetic convective Couette flow of a viscous, electrically conducting and incompressible fluid is studied. The governing equations that describe the flow formation, heat and mass transfer are modeled as Partial Differential Equations (PDEs) and solved numerically using Finite Element Method (FEM). The effect of physical parameters embedded on the velocity, temperature and concentration were studied graphically. It is noticed that, the momentum boundary layer increases as the value of radiation parameter is increased while the velocity of the fluid falls for higher values of the heat sink parameter.

Keywords: Couette flow; radiation; FEM; Heat and mass transfer

Nomenclatures and Greek Symbols

Symbol	Interpretation	Unit
y'	Dimensional length	m
Y	Dimensionless length	
g	Gravitational acceleration	ms^{-2}
k_0	Thermal conductivity	W/mK
T'	Dimensional temperature	K
d	Dimensional channel width	m
T_d'	Ambient temperature	K
u', v'	Dimensional velocity	ms^{-1}
υ	Kinematic viscosity	m^2s^{-1}
C_p	Specific heat at constant pressure	kJ/kgK
Q_0	Volumetric rate of heat generation/absorption	J
S	Constant heat sink parameter	
Pr	Prandtl number	
Sc	Schmidt number	
t'	Dimensional time	s
t	Dimensionless time	
U	Dimensionless velocity	
T	Dimensionless temperature of the fluid	
C	Dimensionless temperature of the fluid	
M	Hatman number	
Rc	Chemical reaction parameter	
Dr	Dufour Number	
β	Coefficient of thermal expansion	$1/K$
β'	Coefficient of thermal expansion	$1/K$
μ	Coefficient of viscosity	Ns/m^2
μ_e	Kinematic viscosity of the fluid	m^2/s
ρ	Fluid density	kg/m^3
σ	Stefan-Boltzman Constant	JK^{-1}

INTRODUCTION

Radiative convective flows are encountered in countless industrial and environmental processes, particularly in astrophysical studies and space technology. Radiative heat and mass transfer play an important role in manufacturing industries for the design of fins, steel rolling, nuclear power plants, gas turbines and various propulsion device for aircraft, combustion and furnace design, materials processing, energy utilization temperature measurements, remote sensing for astronomy and space exploration, food processing cryogenic engineering as well as numerous agricultural, health and military applications. Naik *et al.* (2014) considered thermal radiation effect on an unsteady hydromagnetic free convective oscillatory Couette flow of a viscous fluid embedded in a porous medium. They used a stable finite difference scheme of Crank Nicolson method to obtain their expressions. Omokhuale *et al.* (2019) reported unsteady heat and mass Magnetohydrodynamic (MHD) convective Couette flow with thermal radiation. They solved their problem numerically using FEM. An investigation on the non – linear problem of the effect of Hall current on the unsteady magneto hydrodynamic free convective Couette flow of incompressible, electrically conducting fluid between two parallel plates was carried out, when a uniform magnetic field is applied transverse to the plate, while the thermal radiation, viscous and Joule's dissipation are taken into account. Baoku *et al.* (2010) analyzed magnetic field and thermal radiation effects on steady hydromagnetic Couette flow through a porous channel numerically.

In fluid dynamics, Couette flow refers to the laminar flow of viscous fluid in the space between two parallel plates, one of which moving relative to the other. The flow is driven by virtue of viscous drag force acting on the fluid and the applied pressure gradient parallel to the plates. This type of flow is named in honor of Maurice Marie Alfred Couette, a Professor of Physics at the French University of Angers in the late 19th century. Couette flow is frequently used in undergraduate physics and engineering courses to illustrate shear – driven fluid motion. Some important applications of Couette motion are magnetohydrodynamic power generators and pumps, polymer technology, petroleum industry and purification of crude oil and fluid droplets sprays. The numerical solution of natural convection in unsteady hydromagnetic Couette flow of viscous incompressible electrically conducting fluid between two vertical parallel plates in the presence of thermal radiation was obtained by Rao *et al.* (2014). Mebine (2007) studied the effect of thermal radiation on MHD Couette flow with heat transfer between two parallel plates. The natural convection in unsteady Couette flow of a viscous incompressible fluid confined between two vertical parallel plates in the presence of thermal radiation has been investigated by Narahari (2010). Rajput and Sahu (2012) found the exact solution of natural convection in unsteady hydromagnetic Couette flow of a viscous incompressible electrically conducting fluid between two vertical parallel plates in the presence of thermal radiation.

Finite Element Method (FEM) is a numerical technique used to obtain an approximate solution to boundary value problems as they consist of elliptic partial differential equations and the boundary conditions. It has been applied to many physical problems. The method basically consists of assuming the piecewise continuous function for the solution and obtaining the parameters of the functions in a manner that reduces the error of the solution. Using FEM, Rao *et al.* (2012) examined heat and mass transfer in MHD flow of a viscous fluid past a vertical plate under oscillatory suction velocity. Job and Gunakala (2015) studied unsteady radiative MHD natural convection Couette flow between permeable plates. Raju *et al.* (2016) studied unsteady hydromagnetic natural convection Couette flow of a viscous, incompressible and electrically conducting fluid between two vertical plates in the presence of thermal radiation using finite element method. The entropy generation and temperature dependent heat source effects on MHD Couette flow with permeable base in the presence of radiation and viscous dissipation was studied by Sukumar and Varma (2016). Reddy *et al.* (2017) investigated unsteady MHD heat transfer in Couette flow of water at 4^{O}C in a rotating system with ramped temperature. Ajibade and Bichi (2019) examined natural convection Couette flow through a vertical porous channel due to combined effects of thermal radiation and variable fluid properties. Recently, Bilal *et al.* (2021) worked on Couette flow of viscoelastic dusty fluid in a rotating frame with the heat transfer.

Motivated by the above studies and applications, a novel investigation has been conducted to study unsteady convective Couette flow in the presence of thermal radiation and heat sink. The flow is governed by a modeled coupled nonlinear system of partial differential equations (PDEs) in dimensional form which are transformed into non-dimensional form using some suitable non-dimensional variables. The resulting equations whose exact solutions if possibly found is difficult to get Thus, we numerically used FEM to obtain the solutions. Furthermore, the effects of physical parameters embedded in the problem were examined with the help of graphs.

MATHEMATICAL FORMULATION

The two- dimensional unsteady convective Couette flow of an electrically conducting and viscous fluid between two parallel plates $y = 0$ and $y = d$ surrounded by porous medium under the influence of a uniform transverse magnetic field, thermal radiation and heat source. The following assumptions are considered:

(i) The x' - axis and y' - axis are considered in the vertically upward and normal direction to the plate respectively.

(ii) The plates be separated by a distance d. Initially, at time $t' \leq 0$, the fluid and the plates of the channel are assumed to be at rest and at same temperature T'_d and concentration C'_d. When time $t' > 0$, the plate (at $y' = 0$) begins to move with time dependent velocity $U_0 t'^n$(U_0 is a constant and is a non-negative integer) in its own plane and at the same time the plate temperature and concentration is raised to T'_w and C'_w respectively while the plate (at $y' = d$) is fixed. Similarly, at $t' > 0$, the wall at $y' = d$ is stationary and kept at a constant temperature and concentration T'_d and C'_d respectively.

(iii) The transverse magnetic field of the uniform strength H_0 is to be applied to the plate,

(iv) The fluid has constant suction, kinematic viscosity and thermal conductivity, the Boussinesq approximations has been considered for the flow.

From the above assumptions, the flow is governed by the following PDEs.

Continuity equation:

$$\frac{\partial v^*}{\partial y^*} \tag{1}$$

Momentum equation:

$$v\frac{\partial^2 u^*}{\partial y^{*2}} - \frac{\partial u^*}{\partial t^*} + g\beta_1\left(T^* - T_d^*\right) + g\beta_2\left(C - C_d^*\right) - \frac{\nu u^*}{K^*} - \frac{\sigma\mu_e^2 B_0^2}{\rho}\left(u^* - U_0 t^{*n}\right) = 0 \tag{2}$$

Energy equation:

$$\frac{k_0}{\rho Cp}\frac{\partial^2 T^*}{\partial y^{*2}} - \frac{\partial T^*}{\partial t^*} + \frac{D_m k_T}{c_s c_p}\frac{\partial^2 C^*}{\partial y^{*2}} - \frac{1}{\rho Cp}\frac{\partial q_r}{\partial y'} - Q_0\left(T^* - T_d^*\right) = 0 \tag{3}$$

Species diffusion equation:

$$Dc\frac{\partial^2 C^*}{\partial y^{*2}} - \frac{\partial C^*}{\partial t^*} - Rc\left(C^* - C_d^*\right) = 0 \tag{4}$$

The corresponding initial and boundary conditions are:

$$\left.\begin{aligned} &t^* \le 0 : u^* = 0, T^* = T_d^*, C^* = C_d^* \quad for \quad 0 \le y^* \le d \\ &t^* > 0 : \begin{cases} u^* = U_0 t^{*n}, T^* = T_w^*, C^* = C_w^* \quad at\ y^* = 0 \\ u^* = 0, T^* = T_d^*, C^* = C_d^* \quad at\ \ y^* = d \end{cases} \end{aligned}\right\} \tag{5}$$

The radiative heat flux is reduced by employing the Rosseland approximation given as

$$q_r = -\frac{4\sigma^*}{3k^*}\frac{\partial T^{*4}}{\partial y^*} \tag{6a}$$

we assume that the difference in temperature within the flow are sufficiently small such that q_r may be presented as a linear function of T^*. Therefore, on expanding T^{*4} in Taylor series about T_d^* up to first order approximation, gives

$$T^{*4} = T_d^* + 4\left(T^* - T_d^*\right)T_d^{*3} = 4T^* T_d^{*3} - 3T_d^{*4} \tag{6b}$$

Using Equations (6a) and (6b) in the last term of Equation (2), we have:

$$\frac{\partial q_r}{\partial y^*} = -\frac{16\sigma T_d^{*3}}{3k^*}\frac{\partial^2 T^*}{\partial y^{*2}} \tag{7}$$

Introducing (7) into Equation (2), the energy equation becomes:

$$\frac{\partial T^*}{\partial t^*} = \frac{k_0}{\rho Cp}\frac{\partial^2 T^*}{\partial y^{*2}} + \frac{D_m k_T}{c_s c_p}\frac{\partial^2 C^*}{\partial y^{*2}} + \frac{16\sigma T_d^{*3}}{3k^*\rho Cp}\frac{\partial^2 T^*}{\partial y^{*2}} - Q_0\left(T^* - T_d^*\right) \tag{8}$$

To obtain the non-dimensional form of Equations (1), (3) and (8), the following dimensionless quantities are introduced:

$$\left.\begin{aligned} &U = \frac{u^*}{h}, Y = \frac{y^*}{h}, t = \frac{t^*\nu}{h^2}, T = \frac{T^* - T_h^*}{T_w^* - T_h^*}, C = \frac{C^* - C_h^*}{C_w^* - C_h^*}, \\ &Gr = \frac{g\beta_T\left(T_w^* - T_h^*\right)}{\nu}, Gc = \frac{g\beta_m\left(C_w^* - C_h^*\right)}{\nu}, F = \frac{U_0 h^{2n-1}}{\nu^n} \\ &M^2 = \frac{\sigma\mu_e^2 B_0^2 h^2}{\rho\nu}, R = \frac{3k_0 k^*}{4\sigma T_h^{*3}}, \Pr = \frac{\rho\nu Cp}{k_0}, Sc = \frac{\nu}{D}, \\ &Dr = \frac{D_m k_T h^2\left(C_w^* - C_h^*\right)}{\nu c_s c_p\left(T_w^* - T_h^*\right)}, \mathrm{Re}_x^{-1} = \frac{U_0 x^*}{\nu} \end{aligned}\right\} \tag{9}$$

Using the dimensionless quantities in Equation (9), the dimensionless form of Equations (1), (3) and (8) and (3) are:

$$\frac{\partial^2 U}{\partial Y^2} - \frac{\partial U}{\partial t} + GrT + GcC - M^2\left(U - Ft^n\right) = 0 \tag{10}$$

$$\frac{1}{\Pr}\left(\frac{3R+4}{3R}\right)\frac{\partial^2 T}{\partial Y^2}-\frac{\partial T}{\partial t}+Dr\frac{\partial^2 C}{\partial Y^2}-ST=0 \tag{11}$$

$$\frac{1}{Sc}\frac{\partial^2 C}{\partial Y^2}-\frac{\partial C}{\partial t}-RcC=0 \tag{12}$$

iinitial and boundary conditions (4) in dimensionless forms are:

$$\left.\begin{aligned} &t\le 0: U=0, T=0, C=0 \quad for \quad 0\le Y\le d \\ &t>0: \begin{cases} U=Ft^n, T=1, C=1 \quad at\, Y=0 \\ U=0, T=0, C=0 \quad at\ Y=d \end{cases} \end{aligned}\right\} \tag{13}$$

Two cases are studied, to find the solutions of Equations (10) to (12) subject to the initial and boundary conditions (13):

1. Impulsive movement of the plate at $Y=0$ (i.e., $n=0$) and
2. Uniform accelerated movement of the plate at $Y=0$ (i.e., $n=1$).

Case (1): Impulsive movement of the plate at $Y=0$:

Taking $n=0$ in Equation (10), then the Equation (10) can be expressed as

$$\frac{\partial^2 U}{\partial Y^2}-\frac{\partial U}{\partial Y}+GrT+GcC-M^2\left(U-F\right)=0 \tag{14}$$

and the corresponding boundary conditions (13) reduce to

$$\left.\begin{aligned} &t\le 0: U=0, T=0, C=0 \quad for \quad 0\le Y\le d \\ &t>0: \begin{cases} U=F, T=1, C=1 \quad at\, Y=0 \\ U=0, T=0, C=0 \quad at\ Y=d \end{cases} \end{aligned}\right\} \tag{15}$$

Case (2): Uniform accelerated movement of the plate at $Y=0$.

Taking $n=1$ in Equation (10), then the Equation (10) can be written as

$$\frac{\partial^2 U}{\partial Y^2}-\frac{\partial U}{\partial Y}+GrT+GcC-M^2\left(U-Ft\right)=0 \tag{16}$$

and the initial and boundary conditions (13) reduce to

$$\left.\begin{aligned} &t\le 0: U=0, T=0, C=0 \quad for \quad 0\le Y\le d \\ &t>0: \begin{cases} U=Ft, T=1, C=1 \quad at\, Y=0 \\ U=0, T=0, C=0 \quad at\ Y=d \end{cases} \end{aligned}\right\} \tag{17}$$

For practical engineering applications and the design of chemical engineering systems, quantities of interest viz. Skin-friction, Nusselt and Sherwood numbers which are necessary to compute. The skin-friction or the shear tress at the moving plate of the channel in dimensionless form is given by

$$\tau=-\left(\frac{\tau_w^*}{\rho u_0 \nu}\right)_{y^*=0}=-\left(\frac{\partial U}{\partial Y}\right)_{y^*=0} \tag{18}$$

The rate of heat transfer at the moving hot plate of the channel in dimensionless form is illustrated by

$$Nu_0=-x^*\frac{\left(\frac{\partial T^*}{\partial Y^*}\right)_{y^*=0}}{T_w^*-T_H^*}\Rightarrow Nu_0\,\mathrm{Re}_x^{-1}=-\left(\frac{\partial T}{\partial Y}\right)_{Y=0} \tag{19}$$

Also, the rate of heat transfer on the stationary plate is given by

$$Nu_1=-x^*\frac{\left(\frac{\partial T^*}{\partial Y^*}\right)_{y^*=H}}{T_w^*-T_H^*}\Rightarrow Nu_1\,\mathrm{Re}_x^{-1}=-\left(\frac{\partial T}{\partial Y}\right)_{Y=1} \tag{20}$$

The Sherwood number at the moving plate of the channel in dimensionless form is given by

$$Sh = -x^* \frac{\left(\frac{\partial C^*}{\partial Y^*}\right)_{y^*=0}}{C_w^* - C_H^*} \Rightarrow Sh\,\mathrm{Re}_x^{-1} = -\left(\frac{\partial C}{\partial Y}\right)_{Y=0} \tag{21}$$

where Re_x is the Reynold's number. The mathematical modeling of the problem is now done. So, Equations. (11), (12), (14) and (16) presents a coupled system of linear PDEs and these are to be solved with initial and boundary conditions (15) and (17). Therefore, finding the exact solutions are complicated, whenever it is possible. Thus, these equations are solved numerically by FEM.

Numerical solutions by FEM

The FEM is an efficient numerical and computational method to solving a variety of engineering and real-world problems. So many developers, researchers and users have recognized this method as one of the most powerful numerical analysis tools useful to analyze complex engineering problems. The simplicity, flexibility, computability and accuracy of the method make it significant in modeling and design process. This is because of the discretization of domain of the problem is done employing highly flexible elements or uniform or non-uniform patches that can be easily shown as complex shapes. The method vitally comprises the piecewise continuous functions in a systematic way that reduces the error in the solution.

The steps involved in the finite element analysis as follows:
Step 1: Discretization of the domain
Step 2: Generation of the element equations
Step 3: Assembling of the element equations
Step 4: Imposition of the boundary conditions
Step 5: Solution of assembled equations

Variational Formulation

The Variational formulation associated with Equations (10) to (12) over a typical two-noded linear element (Y_e, Y_{e+1}) is given by

$$\int_{Y_e}^{Y_{e+1}} z_1 \left[\left(\frac{\partial U}{\partial t}\right) - \left(\frac{\partial^2 U}{\partial y^2}\right) - Gr(T) - Gc(C) + M^2\left(U - Ft^n\right)\right] dy = 0 \tag{22}$$

$$\int_{Y_e}^{Y_{e+1}} z_2 \left[\left(\frac{\partial T}{\partial t}\right) - \frac{1}{\mathrm{Pr}}\left(\frac{3R+4}{3R}\right)\left(\frac{\partial^2 T}{\partial y^2}\right) - Dr\left(\frac{\partial^2 C}{\partial y^2}\right)\right] dy = 0 \tag{23}$$

$$\int_{Y_e}^{Y_{e+1}} z_3 \left[\left(\frac{\partial C}{\partial t}\right) - \frac{1}{Sc}\left(\frac{\partial^2 C}{\partial y^2}\right)\right] dy = 0 \tag{24}$$

where z_1, z_2 and z_3 are arbitrary test functions and may be seen as the variation in U, T and C respectively. When the order of integration was reduced, we got the following system of equation:

$$\int_{Y_e}^{Y_{e+1}} z_1 \left[z_1\left(\frac{\partial U}{\partial t}\right) + \left(\frac{\partial z_1}{\partial y^2}\right)\left(\frac{\partial U}{\partial y}\right) + \left(M^2\right)(z_1)U - (F)(z_1)t^n - (Gr)(z_1)T - (Gc)(z_1)C \right] dy$$
$$- \left[\left(z_1\right)\left(\frac{\partial u}{\partial y}\right)\right]_{Y_e}^{Y_{e+1}} = 0 \tag{25}$$

$$\int_{Y_e}^{Y_{e+1}} \left[\left(z_2\right)\left(\frac{\partial T}{\partial t}\right) + \frac{1}{\mathrm{Pr}}\left(\frac{3R+4}{3R}\right)\left(\frac{\partial z_2}{\partial y}\right)\left(\frac{\partial T}{\partial y}\right) + Dr\left(\frac{\partial z_2}{\partial y}\right)\left(\frac{\partial C}{\partial y}\right)\right] dy$$
$$- \left[\left(\frac{z_2}{\mathrm{Pr}}\right)\left(\frac{\partial T}{\partial y}\right) + Dr\left(z_2\right)\left(\frac{\partial T}{\partial y}\right)\right]_{Y_e}^{Y_{e+1}} = 0 \tag{26}$$

$$\int_{Y_e}^{Y_{e+1}} \left[\left(z_3\right)\left(\frac{\partial C}{\partial t}\right) + \frac{1}{Sc}\left(\frac{\partial z_3}{\partial y}\right)\left(\frac{\partial C}{\partial y}\right)\right] dy$$
$$- \left[\left(\frac{z_3}{Sc}\right)\left(\frac{\partial C}{\partial y}\right)\right]_{Y_e}^{Y_{e+1}} = 0 \tag{27}$$

Finite Element Formulation:

The finite element model can be gotten from Equations (25) to (27) by substituting the finite element approximations of the form:

$$U=\sum_{k=1}^{2}U_k^e\xi_k^e, T=\sum_{k=1}^{2}T_k^e\xi_k^e \text{ and } \sum_{k=1}^{2}C_k^e\xi_k^e \tag{28}$$

with $z_1=z_2=z_3=\xi_k^e\ (k=1,2)$, U_k^e, T_k^e and C_k^e are the velocity, temperature and concentration respectively at the k^{th} node of typical e^{th} element (Y_e, Y_{e+1}) and ξ_k^e are the shape functions for this element (Y_e, Y_{e+1}) and are taken as:

$$\xi_1^e=\frac{Y_{e+1}-Y}{Y_{e+1}-Y_e} \text{ and } \xi_2^e=\frac{Y-Y_e}{Y_{e+1}-Y_e},\ Y_e\le Y\le Y_{e+1} \tag{29}$$

This finite element model of the equations for

$$\begin{bmatrix}[P^{11}] & [P^{12}] & [P^{13}]\\ [P^{21}] & [P^{22}] & [P^{23}]\\ [P^{31}] & [P^{32}] & [P^{33}]\end{bmatrix}\begin{bmatrix}\{U^e\}\\ \{T^e\}\\ \{C^e\}\end{bmatrix}+\begin{bmatrix}[W^{11}] & [W^{12}] & [W^{13}]\\ [W^{21}] & [W^{22}] & [W^{23}]\\ [W^{31}] & [W^{32}] & [W^{33}]\end{bmatrix}\begin{bmatrix}\{U'^e\}\\ \{T'^e\}\\ \{C'^e\}\end{bmatrix}=\begin{bmatrix}\{a^{1e}\}\\ \{a^{2e}\}\\ \{a^{3e}\}\end{bmatrix} \tag{30}$$

where $\{\{P^{mn}\},\{W^{mn}\}\}$ and $\{\{U^e\},\{T^e\},\{C^e\},\{U'^e\},\{T^e\},\{C^e\},\{a^{me}\}\}(m=1,2,3)$ are the set of matrices of order 2×2 and 2×1 respectively and $'$ (dash) indicates $\frac{d}{dy}$.

These matrices are defined as follows:

$$P_{Ik}^{11}=\int_{Y_e}^{Ye+1}\left[\left(\frac{\partial\xi_i^e}{\partial y}\right)\left(\frac{\partial\xi_k^e}{\partial y}\right)\right]dy+\left(M^2\right)\int_{Y_e}^{Ye+1}\left[\left(\xi_i^e\right)\left(\xi_k^e\right)\right]dy-Ft^n\int_{Y_e}^{Ye+1}\left(\xi_i^e\right)dy,$$

$$P_{ik}^{12}=-Gr\int_{Y_e}^{Ye+1}\left[\left(\xi_i^e\right)\left(\xi_k^e\right)\right]dy, P_{ik}^{13}=-Gc\int_{Y_e}^{Ye+1}\left[\left(\xi_i^e\right)\left(\xi_k^e\right)\right]dy, W_{ik}^{11}=\int_{Y_e}^{Ye+1}\left[\left(\xi_i^e\right)\left(\xi_k^e\right)\right]dy, W_{ik}^{12}=W_{ik}^{13}=0,$$

$$W_{ik}^{21}, W_{ik}^{23}=0, W_{ik}^{31}=W_{ik}^{32}=0, P_{ik}^{21}=0, P_{ik}^{31}=0, b_i^{1e}=\left[\left(\xi_i^e\right)\left(\frac{\partial U}{\partial Y}\right)\right]_{Y_e}^{Y_{e+1}}$$

$$P_{ik}^{22}=\frac{1}{\Pr}\left(\frac{3R+4}{3R}\right)\int_{Y_e}^{Ye+1}\left[\left(\frac{\partial\xi_i^e}{\partial Y}\right)\left(\frac{\partial\xi_k^e}{\partial Y}\right)\right]dy, P_{ik}^{23}=Du\int_{Y_e}^{Ye+1}\left[\left(\frac{\partial\xi_i^e}{\partial Y}\right)\left(\frac{\partial\xi_k^e}{\partial Y}\right)\right]dy,$$

$$P_{ik}^{33}=\frac{1}{Sc}\int_{Y_e}^{Ye+1}\left[\left(\frac{\partial\xi_i^e}{\partial Y}\right)\left(\frac{\partial\xi_k^e}{\partial Y}\right)\right]dy,\ W_{ik}^{22}\int_{Y_e}^{Ye+1}\left[\left(\xi_i^e\right)\left(\xi_k^e\right)\right]dy,$$

$$a_i^{2e}=\left[\left(\frac{\xi_i^e}{\Pr}\right)\left(\frac{3R+4}{3R}\right)\left(\frac{\partial T}{\partial Y}\right)+Du\left(\xi_i^e\right)\left(\frac{\partial C}{\partial Y}\right)\right]_{Y_e}^{Y_{e+1}}$$

$$a_i^{3e}=\left[\left(\frac{\xi_i^e}{Sc}\right)\left(\frac{\partial C}{\partial Y}\right)\right]_{Y_e}^{Y_{e+1}} \text{ and } W_{ik}^{33}=\int_{Y_e}^{Ye+1}\left[\left(\xi_i^e\right)\left(\xi_k^e\right)\right]dy.$$

In one-dimensional space, linear element, quadratic element or element of higher order can be used. The entire flow domain is divided into 10,000 quadratic elements of equal size. Each element is three-noded, and as such the whole domain contains 20,001 nodes. At each node, three functions are to be evaluated: hence, after assembling of the element equations, we got a system of 80,004 equations which are linear. Thus, an iterative scheme must be employed in the solution. On imposing the boundary conditions, a system of equations was gotten which is solved by Gauss elimination method while maintaining an accuracy of 0.00001. A convergence criterion based on the relative difference between the current and previous iterations is used. After these differences satisfy the desired accuracy, the solution is assumed to have been converged and iterative process terminated. The Gaussian quadrature is implemented for solving the integrations. The code of the algorithm has been executed twice in MAPLE for cases 1 and 2. Excellent results was seen for all results.

Study of grid Independence

In general, to study the grid independency/dependency, the mesh size is varied in order to check the solution at different mesh (grid) sizes and get a range at which there is no variation in the solutions.

RESULTS AND DISCUSSION

A MAPLE program is written to generate line graphs for the velocity, temperature and concentration profiles in other to provide a clear understanding of the problem at hand. Figures 1 and 2 show the effects of thermal and mass Grashof numbers on the velocity profiles. It is seen that, there is rise in the velocity because of the enhancement of thermal buoyancy force. Also, the peak value of the velocity increases rapidly near the porous plate and the decays smoothly for free steam velocity. It is further noted that the fluid velocity increases and the peak value is more distinctive due to increase in species buoyancy force. Thus, the velocity distribution attains a distinctive maximum value in the vicinity of the plate and then reduces properly to approach free stream value. The effect of Magnetic parameter (Hartmann number) on the velocity profiles is as depicted in Figure 3. It is found that, the velocity of the fluid reduces with increasing magnetic parameter. This type of resistive force has a tendency to slow down the flow field. This is due to the fact that the presence of magnetic field in an electrically conducting fluid sets in a force called Lorentz force which acts against the flow if the magnetic field is applied in the normal direction as reflected in the problem.

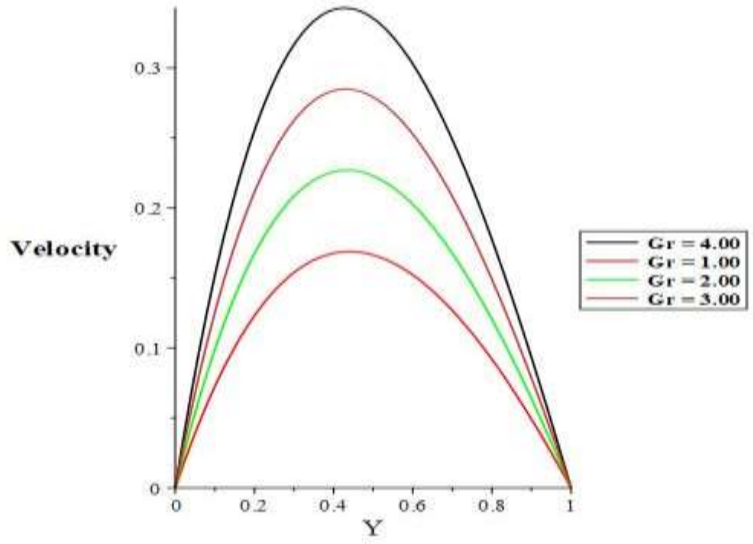

Figure 1: Velocity profiles for different values of Gr.

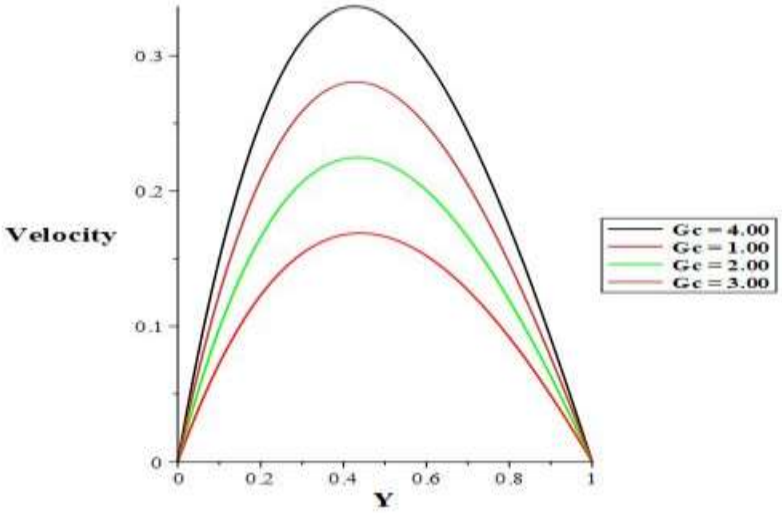

Figure 2: Velocity profiles for different values of Gc.

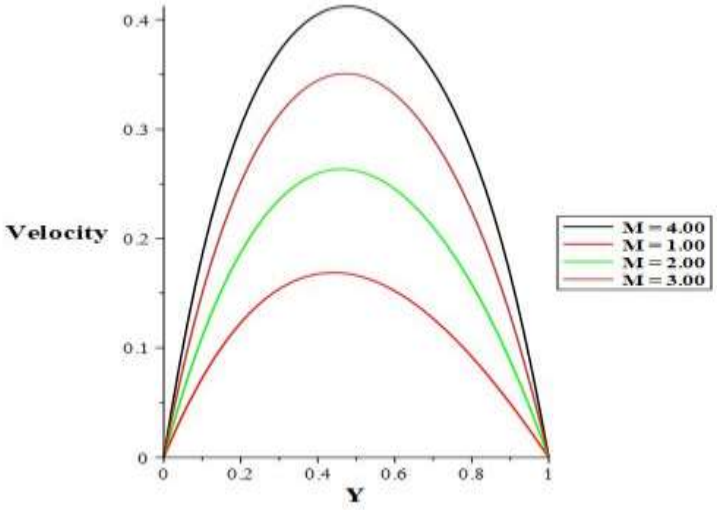

Figure 3: Velocity profiles for different values of M.

It is revealed from Figure 4 that, increase in heat source leads to fall in the fluid velocity profile. Figure 5 describes the effect of Prandtl number on the velocity profiles. From this Figure, it is clear that the velocity become lower as the values of Prandtl number is increased. Physically, this happens due to the phenomenon that fluid with high Prandtl number have greater viscosity, which makes the fluid thick and then move slowly. The effect of Dufour number Du for varied values on the velocity profiles are displayed in Figure 6. It is observed that intensification in Dufour number causes growth in the velocity throughout the boundary layer. However, a distinct velocity overshoot exists near the plate, and thereafter the profiles fall to zero at the edge of the boundary layer. Figures 7 and 8 illustrates the velocity profiles for different values of Schmidt number and thermal radiation parameter. It is noticed that, an increase in Schmidt number results in decrease in the velocity boundary layer while the reverse is seen as thermal radiation becomes significant.

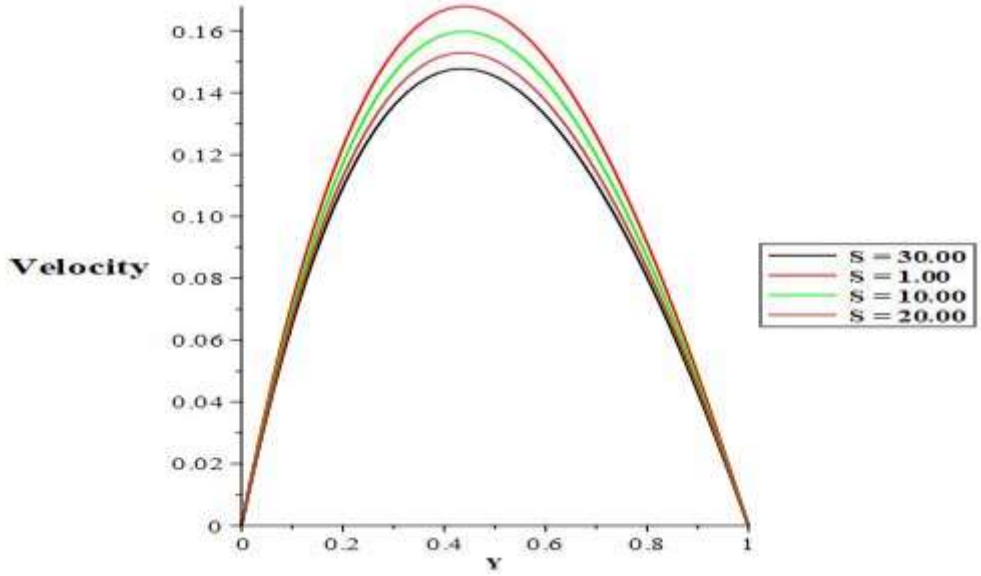

Figure 4: Velocity profiles for different values of S.

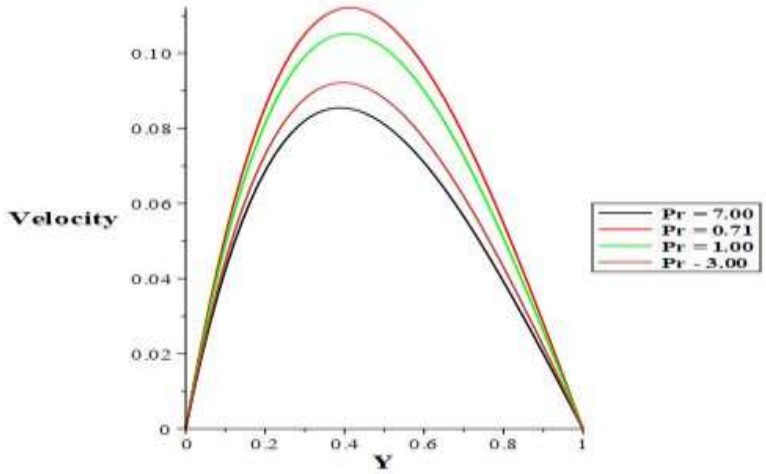

Figure 5: Velocity profiles for different values of Pr.

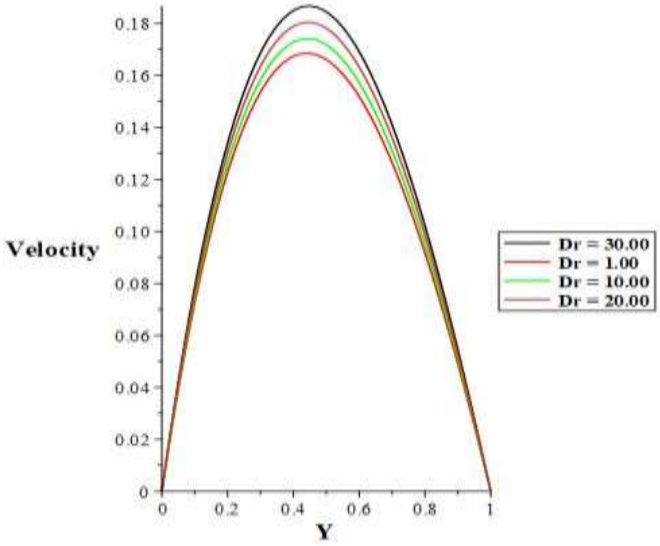

Figure 6: Velocity profiles for different values of Dr.

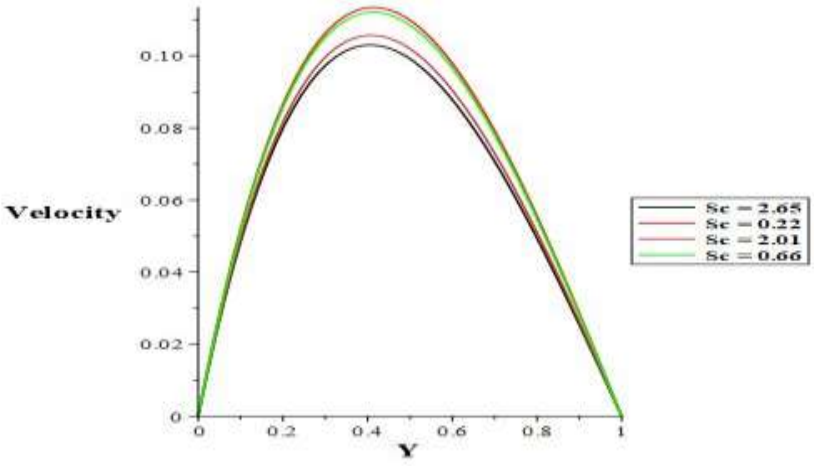

Figure 7: Velocity profiles for different values of Sc.

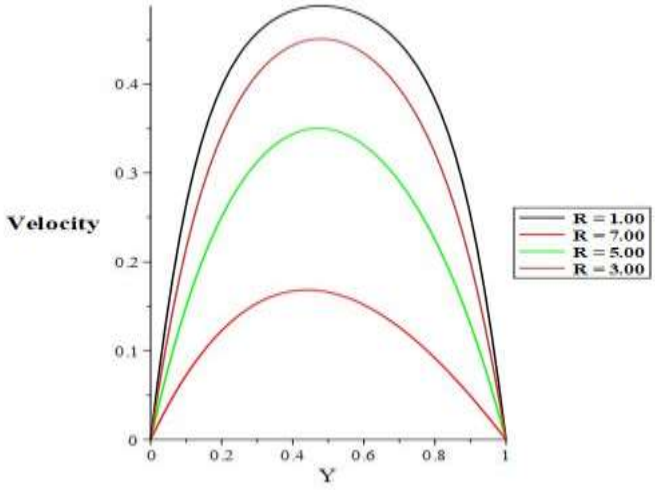

Figure 8: Velocity profiles for different values of R.

Figure 9 presents the effect of Prandtl number on the temperature profiles. From this Figure, it is found that the temperature reduces as Prandtl number is increased. The effect of thermal radiation and heat sink on the velocity profiles in the boundary layer is depicted in Figures 10 and 11. It is noticed that, increase in the thermal radiation parameter results in increasing temperature while a reverse trend is noticed as heat sink becomes higher within the boundary layer.

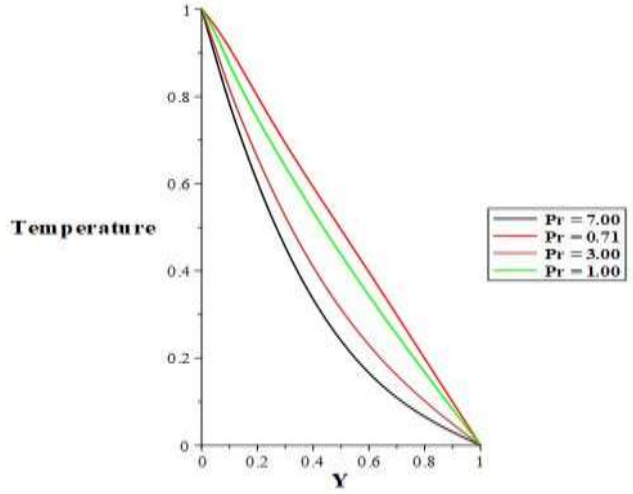

Figure 9. Temperature profiles for different values of Pr.

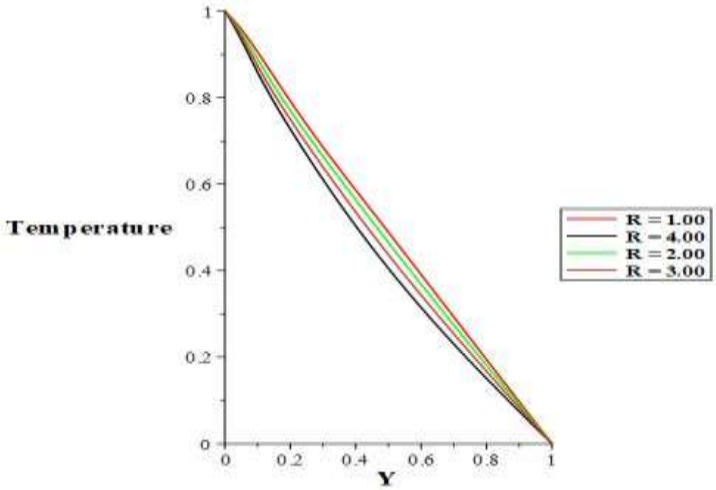

Figure 10: Temperature profiles for different values of R.

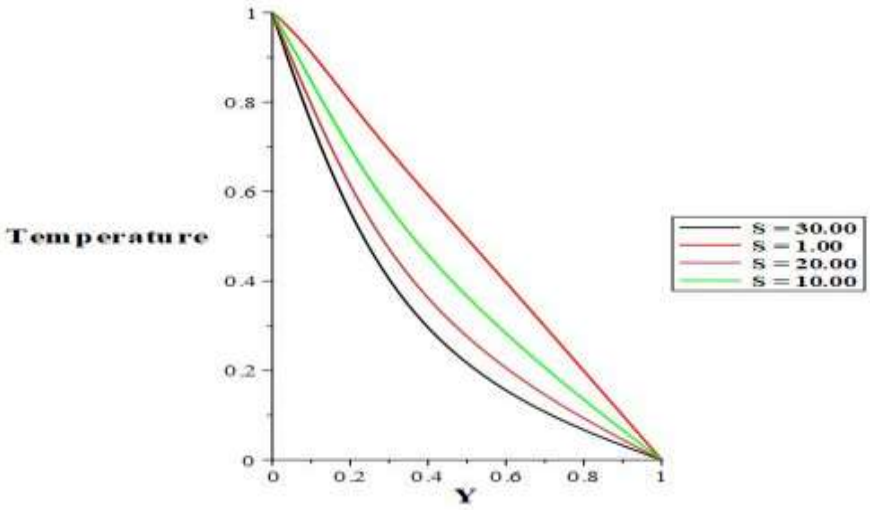

Figure 11: Temperature profiles for different values of S.

Figures 12 and 13 show the concentration field due to variation in Schmidt number and chemical reaction parameter. It is seen that; the concentration of the fluid reduces as the Schmidt number is increased and a similar trend is observed as chemical reaction rises. Physically, this holds because increase in Sc means decrease of molecular diffusivity, which results in decrease of concentration boundary layer. Hence, the concentration of species is smaller for higher values of Sc.

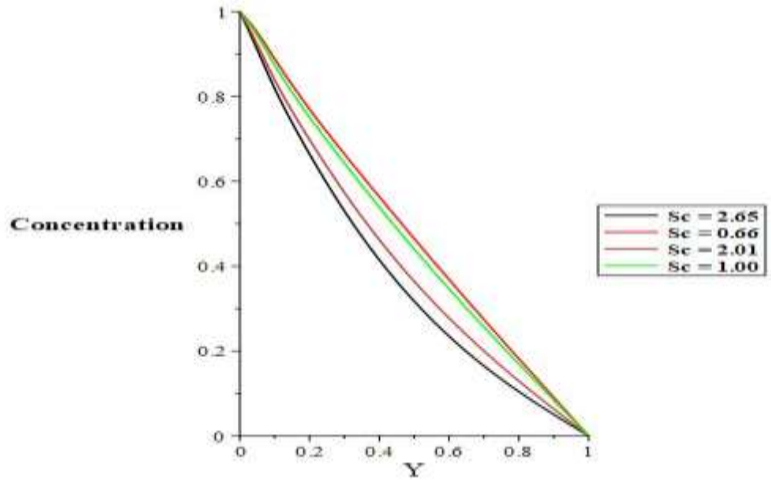

Figure 12: Concentration profiles for different values of Sc.

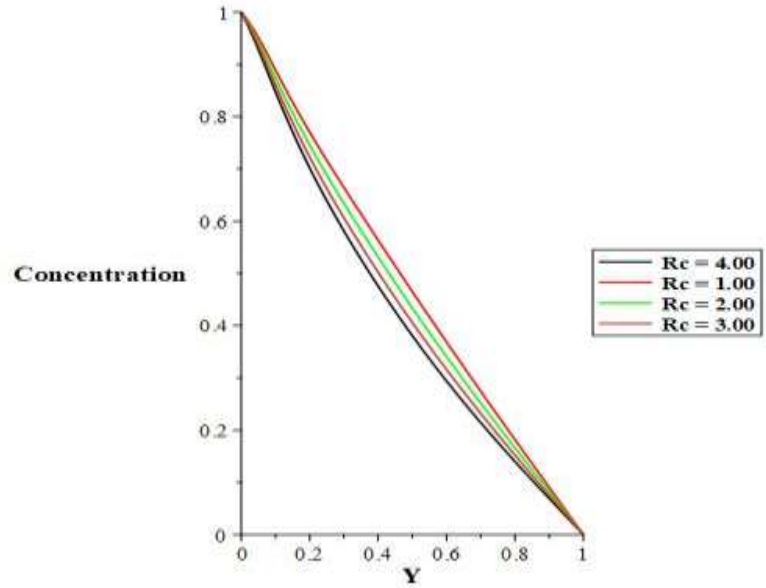

Figure 13: Concentration profiles for different values of *Rc*.

CONCLUSION

We have studied unsteady MHD convective Couette flow with heat sink and radiation effects. The problem is described by a system coupled linear PDEs and solved by FEM. Computations are performed to study the effects of physical parameters on the velocity, temperature and concentration of the fluid. The following conclusion can be drawn from this study:

1. The fluid concentration rises due to higher values of Schmidt number.
2. The momentum boundary layer increases as the value of radiation parameter is increased while the velocity of the fluid falls for higher values of the heat sink parameter.
3. Increasing mass and thermal Grashof numbers boost the velocity profile while the fluid temperature reduces as the value of Prandtl number rises.
4. The velocity of the fluid is boosted significantly when Du is increased. The opposite trend is observed for higher values of M.
5. When the numerical results of the present study are compared with the previous results in literatures with the absence of heat sink and thermal radiation a good agreement was found.

ACKNOWLEDGEMENT

The authors are grateful for the financial support provided by Tertiary Education Trust Fund (TETFund), Nigeria through Federal University Gusau, Nigeria Institutional Based Research (IBR) with grant allocation number "TETF/DR&S/CE/UNIV/GUSAU/IBR/2020/VOL.I".

REFERENCES

Ajibade, A. O. and Bichi, Y. A. (2019). Variable fluid properties and thermal radiation effects on natural convection Couette flow through a vertical porous channel. *Journal of Advances in Mathematics and Computer Science*, 31(1), 1-17.

Baoku, I. G., Israel-Cookey, C. and Olajuwon, B. I. (2010). Magnetic field and thermal radiation effects on steady hydromagnetic Couette flow through a porous channel. *Surveys in Mathematics and its applications*, 5, 215 – 228.

Bilal, M., Khan, S., Ali, F., Arif, M., Khan, I. and Nisar, K. S. (2021). Couette flow of viscoelastic dusty fluid in a rotating frame along with the heat transfer. *Scientific Reports*, 11(506), 1 – 16.

Job, V. M., and Gunakala, S. R. (2015). Finite element analysis of unsteady radiative MHD natural convection Couette flow between permeable plates with viscous and joule dissipation. *International Journal of Pure and Applied Mathematics*, 99(2), 123 – 143.

Mebine, P. (2007). Radiation effects on MHD Couette flow with heat transfer between two parallel plates. *Global Journal of Pure and Applied Mathematics*, 3(2), 191 – 202.

Naik, S. H., Rao, K. R. and Murthy, M. V. (2014). Thermal radiation effect on an unsteady hydromagnetic free convective oscillatory Couette flow of a viscous fluid embedded in a porous medium. *International Journal of Emerging Trends & Technology in Computer Science*, 3(4), 6 – 12.

Omokhuale, E., Altine, M. M. and Yusuf, A. (2019). Unsteady heat and mass transfer Magnetohydrodynamic (MHD) convective Couette flow with thermal radiation using FEM. *Caliphate Journal of Science and Technology*, 1, 61 – 70.

Naik, S. H., Murthy, M. V. R. and Rao, K. R. (2014). The effect of Hall current on an unsteady MHD free convective Couette flow between two permeable plates in the presence of thermal radiation. International Journal of Computational Engineering and Research, 4(7), 40 – 55.

Narahari, M. (2010). Effects of thermal radiation and free convection currents on unsteady Couette flow between two vertical parallel plates with constant heat flux at one boundary. *WSEAS Transactions on Heat and Mass Transfer*, 5, 21 – 30.

Rajput, U. S. and Sahu, P. K. (2012). Natural convection in unsteady hydromagnetic Couette flow through a vertical channel in the presence of thermal radiation. *International Journal of Pure and Applied Mechanics*, 8(3), 35 – 56.

Raju, R. S., Reddy, G. J., Rao, J. A. and Rashidi, M. M. (2016). Thermal diffusion and diffusion thermo effects on an unsteady heat and mass transfer Magnetohydrodynamic natural convection Couette flow using FEM. *Journal of Computational Design and Engineering*, 3, 349 – 362.

Rao, K. R., Murthy, M. V. R. and Naik, S. Hari singh (2014). Thermal radiation effect on an unsteady MHD natural convection Couette flow with heat and mass transfer. *International Journal of Computers and Technology*, 12(8), 3786 – 3802.

Reddy, G. J., Raju, R. S., Rao, J. A. and Gorla, R. S. R. (2017). Unsteady MHD heat transfer in Couette flow of water at 4°C in a rotating system with ramped temperature via finite element method. *International Journal of Applied Mechanics and Engineering*, 22(1), 145 – 161.

Sukumar, M. and Varma, S. V. K. (2016). Entropy generation and temperature dependent heat source effects on MHD Couette flow with permeable base in the presence of radiation and viscous dissipation. *Middle-East Journal of Scientific Research*, 24 (8), 2577 – 2588.